

Turbulent Characteristics of Saltation and Uncertainty of Saltation Model Parameters

Dongwei Liu¹, Masahide Ishizuka², Masao Mikami³, Yaping Shao^{4*}

¹School of Ecology and Environment, Inner Mongolia University, China

liudw@imu.edu.cn

²Faculty of Engineering, Kagawa University, Japan

ishizuka@eng.kagawa-u.ac.jp

³Office of Climate and Environmental Research Promotion, Japan Meteorological Business Support Center, Japan

mikami@jmbc.or.jp

⁴Institute for Geophysics and Meteorology, University of Cologne, Germany

yshao@uni-koeln.de

Abstract: It is widely recognized that saltation is a turbulent process, similar to other transport processes in the atmospheric boundary layer. Due to lack of high frequency observations, the statistic behavior of saltation is so far not well understood. In this study, we use the data from the Japan-Australian Dust Experiment (JADE) to investigate the turbulent characteristics of saltation by analyzing the probability density function, energy spectrum and intermittency of saltation fluxes. Threshold friction velocity, u_{*t} , and saltation coefficient, c_0 , are two important parameters in saltation models, often assumed to be deterministic. As saltation is turbulent in nature, we argue that it is more reasonable to consider them as parameters obeying certain probability distributions. We estimate these distributions using the JADE data. The factors contributing to the stochasticity of u_{*t} and c_0 are examined.

Keywords: wind erosion; turbulent saltation; saltation intermittency; saltation model; threshold friction velocity; saltation coefficient; maximum likelihood

Highlight: We use data from a field experiment to study saltation by analysing the probability density function, energy spectrum and intermittency of saltation fluxes. We also estimate two key wind-erosion model parameters and their probabilistic distributions. It continues the line of treating saltation as a turbulent process and represents a progress towards deriving more general wind erosion models.

1. Introduction

It is well-recognised that saltation, the hopping motion of sand grains near the earth's surface, is a turbulent process [Bagnold, 1941]. However, early studies focused mainly on its "mean" behaviour. Most well-known is, for example, the Owen [Owen, 1964] saltation model which predicts that the vertically integrated saltation flux is proportional to u_* cubed, where u_* is friction velocity, defined as $u_* = \sqrt{\tau / \rho}$ with τ being surface shear stress (N m^{-2}) and ρ air density (kg m^{-3}). A dedicated investigation on turbulent saltation was conducted by Butterfield [1991], which revealed the significant variability of saltation fluxes concealed in conventional time-averaged data. Stout and Zobeck [1997] introduced the idea of saltation intermittency and pointed out that even when the averaged u_* is below the threshold friction velocity, u_{*t} , saltation can still intermittently occur. The latter authors emphasized on saltation intermittency caused by fluctuations of turbulent wind, but stochasticity of u_{*t} can also play a role. Turbulent saltation has attracted much attention in more recent years [e.g. McKenna Neuman et al. 2000; Davidson-Arnott and Bauer, 2009; Sherman et al. 2017] and large-eddy simulation models have been

48 under development to model the process [e.g. Dupond et al. 2013]. However, due to a lack of
 49 high-frequency field observations of saltation fluxes, the statistical behaviour of turbulent
 50 saltation is, to date, not well understood.

51 A related problem is how saltation can be parameterized in wind erosion models. For example,
 52 for dust modelling, it is important to quantify saltation, as saltation bombardment is a main
 53 mechanism for dust emission. In wind erosion models, u_{*t} is a key parameter which depends on
 54 many factors including soil texture, moisture, salt concentration, crust and surface roughness.
 55 In models, it is often expressed as

$$56 \quad u_{*t}(d; \lambda, \theta, s_l, c_r, \dots) = u_{*t}(d) f_\lambda(\lambda) f_\theta(\theta) f_{s_l}(s_l) f_{c_r}(c_r) \dots \quad (1)$$

57 where $u_{*t}(d)$ is the minimal threshold friction velocity for grain size d [Shao and Lu, 2000]; λ is
 58 roughness frontal-area index; θ is soil moisture; s_l is soil salt content and c_r is a descriptor of
 59 surface crustiness; f_λ , f_θ , f_{s_l} and f_{c_r} are the corresponding correction functions. The corrections
 60 are determined semi-empirically, e.g., f_λ using the Raupach et al. [1993] scheme and f_θ the Fécan
 61 et al. [1999] scheme. The corrections f_{s_l} and f_{c_r} are so far not well known.

62 For homogeneous saltation, the saltation flux can be computed using the Kawamura [1964]
 63 scheme, here multiplied by the fraction of erodible surface area σ_f ,

$$64 \quad Q(d) = \begin{cases} \sigma_f c_0 \frac{\rho}{g} u_*^3 \left(1 - \frac{u_{*t}}{u_*}\right) \left(1 + \frac{u_{*t}}{u_*}\right)^2 & u_* > u_{*t} \\ 0 & u_* \leq u_{*t} \end{cases} \quad (2)$$

65 where d is particle diameter in sand particle size range and g is acceleration due to gravity. The
 66 saltation coefficient, c_0 , is usually estimated empirically from field and/or wind-tunnel
 67 experiments. It falls between 1.8 and 3.1 according to Kawamura [1964], and is commonly set
 68 to 2.6 [White, 1979] in wind erosion models. The total (all particle sizes) saltation flux, Q , is a
 69 particle-size weighted average of $Q(d)$

$$70 \quad Q = \int_{d_1}^{d_2} Q(d) p_s(d) \delta d \quad (3)$$

71 where d_1 and d_2 define the upper and lower limits of saltation particle size, respectively, and
 72 $p_s(d)$ is the soil particle size distribution. Observations show, however, c_0 varies considerably
 73 from case to case (e.g. Gillette et al. 1997; Leys, 1998), and as the data presented later in this
 74 paper show, for a given location, it may vary from day to day and even during a wind erosion
 75 event.

76 While wind-erosion modules built in numerical weather and global climate models [e.g. Shao
 77 et al. 2011; Kok et al. 2014; Klose et al. 2014] are in general more sophisticated than what is
 78 described above and include a dust emission scheme, the estimate of Q is essentially done using
 79 Equations (1) to (3) or similar. Thus, the estimates of u_{*t} and specification of c_0 are critical to
 80 wind-erosion and dust modelling.

81 In most wind erosion models, both u_{*t} and c_0 are treated as being deterministic. As saltation is
 82 turbulent, it is more rational to treat u_{*t} and c_0 as parameters that satisfy certain probability

92 distributions. Saltation intermittency also implies that u_{*t} and c_0 depend on the scale of
 93 averaging. Shao and Mikami [2005] noticed that u_{*t} for 10-minute averaged Q and 1-minute
 94 averaged Q are quite different. Namikas et al. [2003] and Ellis et al. [2012] have also noticed
 95 that averaging intervals of surface shear stress are important to quantifying sediment transport
 96 because both shear stress and saltation flux are turbulent.

97
 98 Between 23 Feb and 14 Mar 2006, Ishizuka et al. (2008; 2014) carried out the Japan-Australian
 99 Dust Experiment (JADE) in Australia. In JADE, both u^* and Q , together with a range of
 100 atmospheric and soil surface quantities, were measured at relatively high sampling rates. The
 101 loamy sand soil surface at the JADE site was very mobile and thus the JADE data are
 102 representative to surfaces almost ideal for sand drifting. In this study, we analyse some aspects
 103 of the turbulent behaviour of saltation using the JADE measurements of saltation fluxes. In light
 104 of the analysis, we ask the question what the most likely values of u_{*t} and c_0 are and how
 105 representative they are. We also estimate the probability distribution of the two parameters.

107 2. Data and Method for Parameter Estimation

109 2.1 JADE Data

110
 111 Ishizuka et al. carried out JADE between 23 Feb and 14 Mar 2006 on an Australian farm at
 112 (33°50'42.4"S, 142°44'9.0"E). The size of field is about 1 km in the E–W direction and about
 113 4 km in the N–S direction. A range of atmospheric variables, land surface properties, soil
 114 particle-size distributions and size-resolved sand and dust fluxes were measured. During the
 115 study period, 12 wind-erosion episodes were recorded. The dataset is particularly valuable in
 116 that particle size resolved sand and dust fluxes [Shao et al. 2011] were measured. The details
 117 of the experiments and datasets can be found in Ishizuka et al. [2008, 2014] and hence only a
 118 brief summary is given here.

119
 120 In JADE, three Sand Particle Counters (SPCs) [Yamada et al. 2002] were used to measure
 121 saltation at the 0.05, 0.1 and 0.3 m levels with a sampling rate of 1 Hz. A SLD (Super
 122 Luminescent Diode) light source is used to detect particles flying through the light beam. The
 123 frequency of the input signal is 1-30 kHz, implying that particles moving with speed less than
 124 30 m s^{-1} can be detected. A SPC measures the saltation of particles in the range of 39 - 654 μm
 125 in 32 bins with mean diameters of 39, 54, 69 μm etc. with irregular increment ranging between
 126 15 and 23 μm . At each measurement height, the saltation flux density ($\text{M L}^{-2} \text{T}^{-1}$), q , is obtained
 127 as the sum of q_j (saltation flux for size bin j) for the 32 size bins, i.e.

$$129 \quad q = \sum_{j=1}^{32} q_j \quad (4)$$

130 The saltation flux, Q , is then estimated by integrating q over height, namely,

$$132 \quad Q = \int q dz \quad (5)$$

133
 134 In computing Q , we assume $q = q_0 \exp(-az)$ with q_0 and a being fitting parameters from the
 135 measurements. Prior to the field experiment, the SPCs were calibrated in laboratory and during
 136 JADE, they were checked in a mobile wind-tunnel at the site and compared with other saltation
 137 samplers. But as q was measured only at three heights, the vertical resolution of q is relatively
 138 poor and inaccuracies in the Q estimates are unavoidable, which we are unable to fully quantify.

139 However, the profiles of q are well behaved and thus the inaccuracies in the absolute values of
140 the Q estimates are not expected to be so large as to affect the conclusions of this study.

141
142 Q is computed using the SPC data at 1-second intervals. We denote its time series as Q_{1sec} .
143 From Q_{1sec} , the one-minute averages, Q_{1min} , and 30-minute averages of saltation fluxes, Q_{30min} ,
144 are derived. All these quantities are also computed for individual particle size bins as

$$145 \quad Q_j = \int q_j dz \quad (5a)$$

147
148 Atmospheric variables, including wind speed, air temperature and humidity at various levels,
149 as well as radiation, precipitation, soil temperature and soil moisture were measured using an
150 automatic weather station (AWS). These quantities were sampled at 5-second intervals and their
151 averages over 1-minute intervals were recorded. Two anemometers were mounted at heights
152 0.53 m and 2.16 m on a mast for measuring wind speed. Also available are the Monin-Obukhov
153 length and sensible heat fluxes. From the wind measurements, surface roughness length z_0 and
154 friction velocity u_* are derived, assuming a logarithmic profile (with stability correction) of the
155 mean wind. The roughness length for the experiment site is estimated to be 0.48 mm.

156
157 Friction velocity is computed with 1-minute averaged wind data, denoted as u_{*1min} , and 30-
158 minute averaged wind data, denoted as u_{*30min} . In atmospheric boundary-layer studies, there is
159 no standard for how long one should average wind to “correctly” estimate u_* , but it is common
160 to average over 10 to 30 minutes. But how long one averages depends on the purpose of the
161 averaging. If u_* is used as a scaling velocity for the atmospheric boundary layer, e.g., as measure
162 of turbulence intensity, it is necessary to average over a sufficiently large time interval to obtain
163 a “constant” u_* . In this paper, u_* is a surrogate of shear stress, the variation of which drives that
164 of saltation. Therefore, short averaging times are preferred, subject to that they are larger than
165 the response time of aeolian flux to shear stress. Anderson and Haff (1988) and Butterfield
166 (1991) suggested that this response time is of order of one second.

167
168 Observations of surface soil properties, including soil temperature and soil moisture, were made
169 at 1-minute intervals. The surface at the JADE site was relatively uniform. A survey of ground
170 cover over an area of 900 x 900 m² at the site was made on 11 March 2006. The area was
171 divided into 9 tiles and surveyed along one transect of 300 m long in each tile. Photographs
172 were taken every 5 m by looking down vertically to a point on the ground. Surface cover was
173 estimated to be ~ 0.02 (see Appendix of Shao et al. 2011).

174
175 The wind erosion model, as detailed in Shao et al. (2011), is used for computing the saltation
176 fluxes using the JADE atmospheric and surface soil measurements as input. The saltation model
177 component is as described in Section 1, consisting of Equations (1) – (3). The fraction of
178 erodible surface area, σ_f , used in Equation (1), is one minus the fraction of surface cover. The
179 soil particle size distribution (psd), $p_s(d)$, required for Equation (3), is based on soil samples
180 collected at the JADE site and analyzed in laboratory. The analysis was done using a Microtrac
181 (Microtrac MT3300EX, Nikkiso Co. Ltd.), a particle size analyzer based on laser diffraction
182 light scattering technology. Water was used for sample dispersion. Depending on the methods
183 (pretreatment and ultrasonic vibration) used, the soil texture can be classified as sandy loam
184 (clay 0.3%, silt 25% and sand 74.7%) or loamy sand (clay 11%, silt 35% and sand 54%). The
185 sandy loam psd is used in this study, which has a mode at ~180 μm (see Shao et al. 2011, Fig.
186 5, Method A).

187

188 The default value of c_0 is set to 2.6, as widely cited in the literature [e.g. White, 1979] and the
 189 default value of u_{*t} is computed using Equation (1) with $u_{*t}(d)$ computed using the Shao and Lu
 190 [2000] scheme, f_λ using the Raupach et al. [1993] scheme, f_θ the Fécan et al. [1999] scheme,
 191 and f_{sl} and f_{cr} set to one. The frontal area index λ and soil moisture θ are both observed data
 192 from JADE.

193

194 **2.2 Method for Parameter Estimation**

195

196 Different choices of c_0 and u_{*t} would lead to different model-simulated saltation fluxes which
 197 may or may not agree well with the measurements. By fitting the simulated saltation fluxes to
 198 the measurements, we determine the optimal estimates of c_0 and u_{*t} and the probability density
 199 function (pdf) of these parameters. The method based on the Bayesian theory is used for the
 200 purpose.

201

202 Suppose $\tilde{X} = (\tilde{x}_1, \tilde{x}_2, \dots, \tilde{x}_n)$ is a measurement vector, with \tilde{x}_i being the measured value at time t_i ,
 203 and A is a model with a forcing vector F and model parameter vector β . Let the initial state of
 204 the system be i_0 , then the modelled value of the system, $X = (x_1, x_2, \dots, x_n)$, can be expressed as

205

$$206 \quad X(\beta) = A(i_0, F; \beta) \quad (6)$$

207

208 The error vector is given by $E(\beta) = \tilde{X} - X$, here, fully attributed to β . Given \tilde{X} , the posterior
 209 parameter pdf, $p(\beta|\tilde{X})$, can be estimated from the Bayes theorem:

210

$$211 \quad p(\beta|\tilde{X}) \propto p(\beta)p(\tilde{X}|\beta) \quad (7)$$

212

213 where $p(\beta)$ is the prior parameter pdf and $p(\tilde{X}|\beta)$ the likelihood. If $p(\beta)$ is given, then the
 214 problem of finding $p(\beta|\tilde{X})$ reduces to finding the maximum likelihood. Assuming the error
 215 residuals are independent and Gaussian distributed with constant variance, σ^2 , the likelihood
 216 can be written as

217

$$218 \quad p(\tilde{X}|\beta) = \prod_{i=1}^n \frac{1}{\sqrt{2\pi}\sigma} \exp\left(-\frac{(x_i - \tilde{x}_i)^2}{2\sigma^2}\right) \quad (8)$$

219

220 In this case, maximizing the likelihood is equivalent to minimizing the error, i.e.,

221

$$222 \quad R^2(\beta) = \min \sum_i (x_i - \tilde{x}_i)^2 \quad (9)$$

223

224 The solution of Equation (9) gives an optimal (i.e. with maximum likelihood) estimate of mean
 225 β . This is the popular least-squares method. A disadvantage of the method is that it assumes a
 226 Gaussian posterior parameter pdf and the computing the β variance requires the pre-knowledge
 227 of the accuracy of the data.

227

228 As an alternative, the approximate Bayesian computation (ABC) method has been proposed
 229 [e.g. Vrugt and Sadegh, 2013]. It is argued that a parameter value β^* should be a sample from

230 $p(\beta|\tilde{X})$ as long as the distance between the observed and simulated data is less than a small
231 positive value

232

$$233 \rho(\beta^*) = |X(\beta^*) - \tilde{X}| \leq \varepsilon \quad (10)$$

234

235 This procedure provides explicitly an estimate of parameter pdf for given dataset. The ABC
236 method is numerically simple: from a prior pdf (e.g. uniform) of β a β^* is stochastically
237 generated and the model is run. If Equation (10) is satisfied, then β^* is accepted or otherwise
238 rejected. This procedure is repeated and the a-priori pdf of β is mapped to a posterior pdf of β .
239 The ABC method has the disadvantage though that it is numerically inefficient. More efficient
240 techniques based on the same principle exist, e.g., Markov Chain Monte Carlo Simulation
241 [Sadegh and Vrugt, 2014]. In this study, we apply the Differential Evolution Adaptive
242 Metropolis (DREAM) algorithm proposed by Vrugt et al. (2011) for estimation of hydrologic
243 model parameters. The algorithm integrates Differential Evolution [Storn and Price, 1997] and
244 self-adaptive randomized subspace sampling to accelerate a Markov Chain Monte Carlo
245 simulation. A full description of the DREAM algorithm is beyond the scope of our study.
246 Interested readers should refer to the above cited references for details.

247

248 **3. Statistical Features of Saltation**

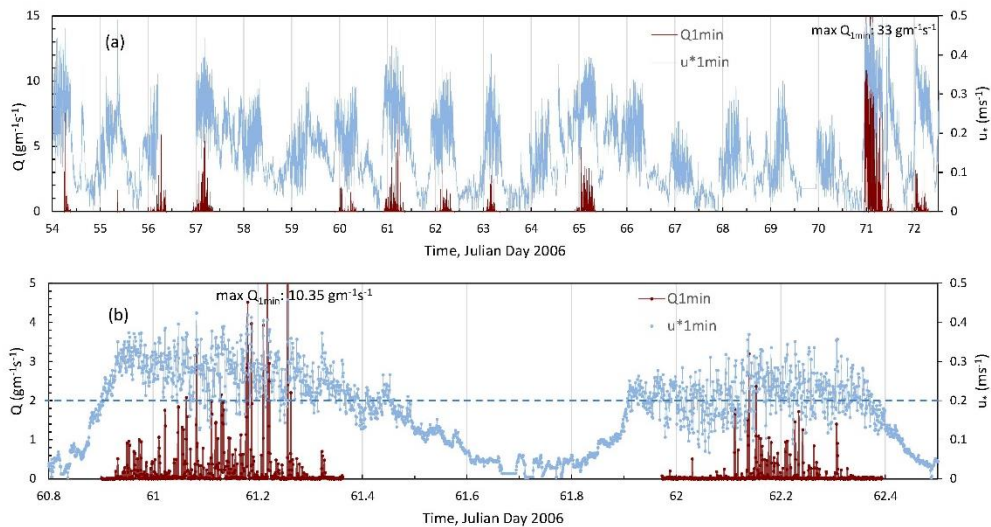
249

250 **3.1 Time Series**

251

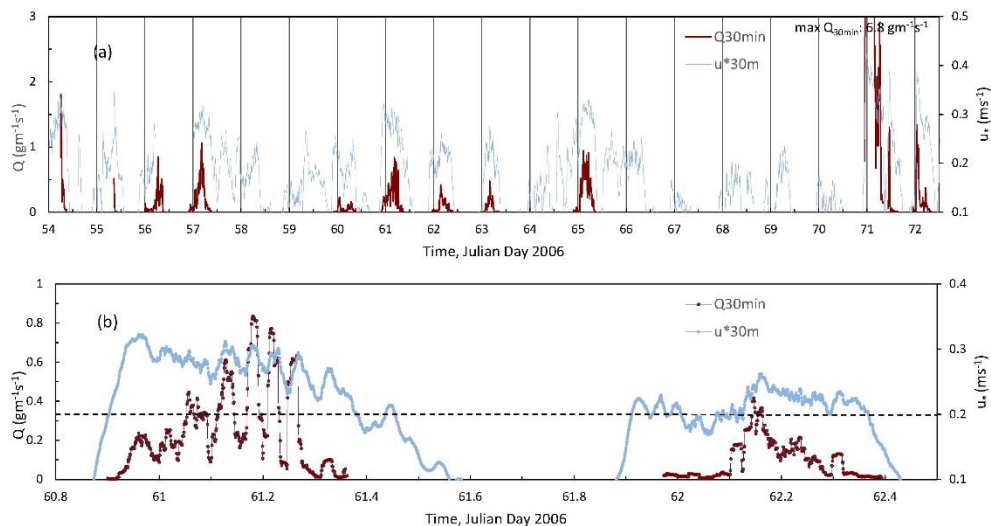
252 To provide an overview of the dataset used in this study. Fig. 1a shows the time series of Q_{1min}
253 and u^*_{1min} , and Fig. 2 Q_{30min} and u^*_{30min} . During the 20-day period, aeolian sand drift occurred
254 almost every day at the site according to the field logging book, but only 12 events were
255 recorded using the SPCs. Saltation fluxes were not measured on Day 55, 58, 59, 64 and then
256 Day 66 to 70, due to either instrument maintenance or use of the SPCs for other purposes (e.g.
257 wind-tunnel experiments). The figures show that both Q and u^* fluctuate significantly and
258 saltation is turbulent. Fig. 1b shows an enlarged plot of the Q_{1min} and u^*_{1min} time series for Day
259 61 and 62. At the JADE site, u^*_t was about 0.2 m s^{-1} . On Day 61, u^* was mostly larger than this
260 value and saltation was almost continuous, while on Day 62, u^* was close to this value and
261 weak saltation occurred frequently also when u^* was below 0.2 m s^{-1} . Fig. 2b is as Fig.1b, but
262 for Q_{30min} and u^*_{30min} . A comparison of Fig. 1b and Fig. 2b reveals that the amplitude of the
263 Q_{1min} fluctuations is several times of that of the Q_{30min} fluctuations. A strong correlation between
264 the time series of Q_{30min} and u^*_{30min} can be directly seen in Fig. 2b.

265



266
267
268
269
270
271

Figure 1: (a) Observed time series of 1-min averaged saltation flux, Q_{1min} ($\text{g m}^{-1} \text{s}^{-1}$), and friction velocity, u^*_{1min} (m s^{-1}), for the JADE study period; (b) an enlarged plot of (a) for the erosion events on Day 61 and 62. Note that the axes in (b) have different scales than in (a).



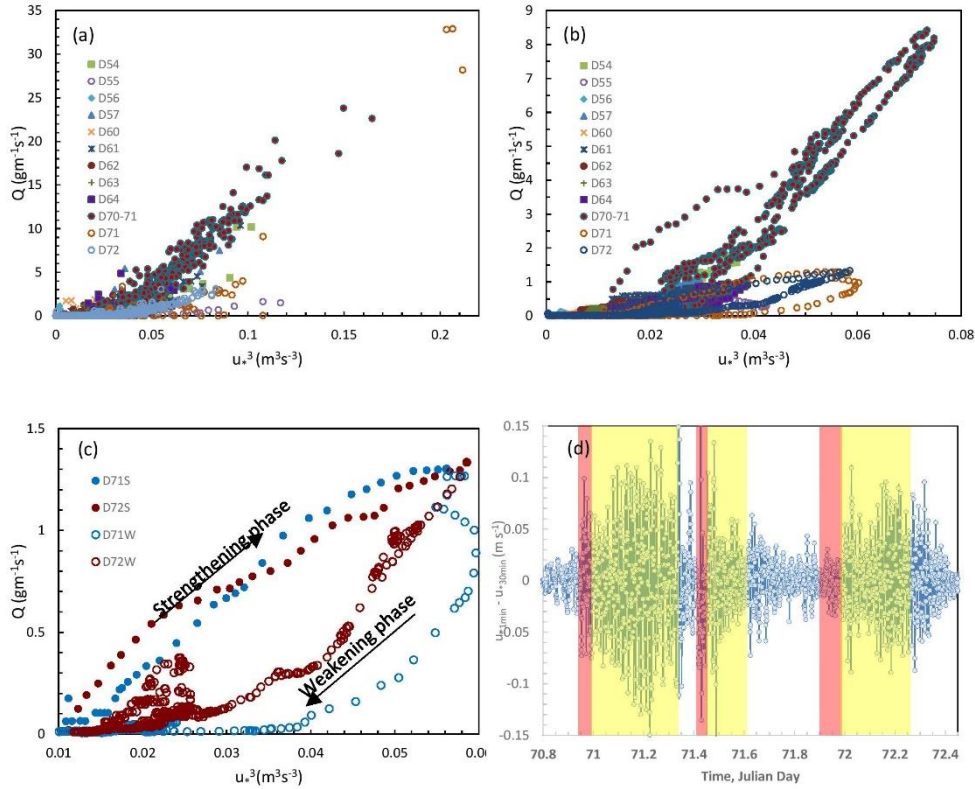
272

273 Figure 2: As Fig. 1, but for running means over 30-min intervals.

274

275 In Fig. 3a, b and c, Q is plotted against u_*^3 . Several interesting features can be identified. For
276 the majority of the points, the $Q \sim u_*^3$ relationship appears to hold, but this relationship can vary
277 significantly even for the same data set from event to event. For example, large differences exist
278 between days 70 and 71 (denoted D70-71, an event of intensive wind erosion) and Day 72 (a
279 day of weak wind erosion), as seen in both Fig. 3a and Fig. 3b. There may be many likely
280 reasons for the differences the $Q \sim u_*$ relationship but the most conspicuous are differences in
281 atmospheric turbulence (e.g., gustiness) and time-varying surface conditions (e.g. particle
282 sorting and aerodynamic roughness). Fig. 3d shows the time series of $(u^*_{1min} - u^*_{30min})$, a measure
283 of turbulent fluctuations. It is seen that saltation is associated with not only high surface shear
284 stress but also high shear stress fluctuations. The large difference in the $Q \sim u_*$ relationship
285 between D70-71 and D72 (Fig. 3b) is probably attributed to the strong differences in turbulent
286 fluctuations (Fig. 3d): D70-71 was a hot gusty day with top (2 cm) soil temperature reaching
287 53°C , while D72 was cooler and less gusty with soil temperature 5°C lower. Also hysteresis is

288 observed in the $Q \sim u_*$ relationship, as shown in Fig. 3c, using D71 and D72 as example. Fig. 3d
 289 shows that for all three events selected (D70-71, D71 and D72), saltation has a relatively short
 290 (0.5 to 2 hours) strengthening phase, followed by a longer weakening phase. During an erosion
 291 event, for the same u_* , saltation is stronger in the strengthening than in the weakening phase.
 292 An examination of Fig. 3d suggests that the hysteresis cannot be simply attributed to the
 293 intensity of turbulence. We speculate that it is probably more related to flow-saltation feedbacks
 294 (e.g. stronger splash entrainment in the strengthening phase) and the modification of surface
 295 aerodynamic conditions (e.g. particle sorting and reduced surface roughness Reynolds number).
 296



297

298 Figure 3: (a) Saltation flux, Q ($\text{g m}^{-1} \text{s}^{-1}$), plotted against friction velocity, u_*^3 ($\text{m}^3 \text{s}^{-3}$), for 1-
 299 minute averages; (b) As (a), but for 30-minute averages; (c) As (b), but enlarged to illustrate
 300 saltation hysteresis on D71 and 72; D71S/72S denote the strengthening and D71W/72W the
 301 weakening phase of the D71/72 event; (d) Time series of u_* derivations, given by $(u_*1_{min} - u_*30_{min})$,
 302 for D70-71, D71 and D72. The strengthening phase is marked red and the weakening phase
 303 yellow.

304

305 3.2 Probability Density Function of Saltation Fluxes

306

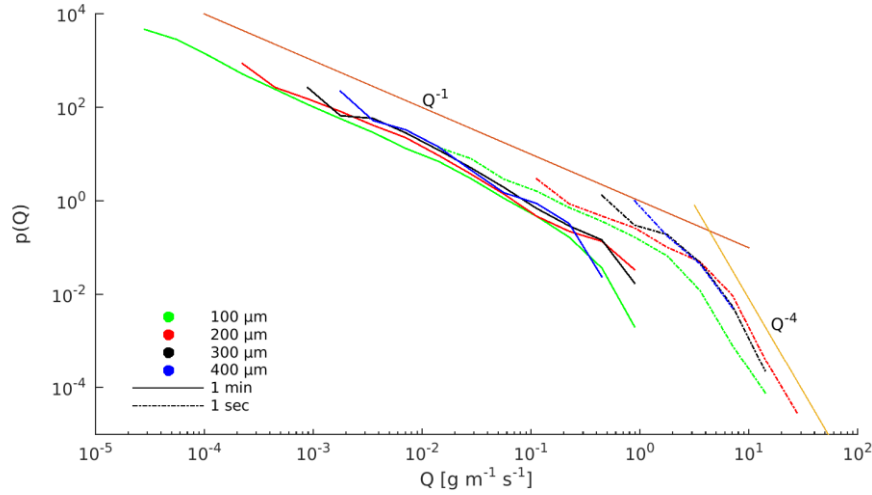
307 How well the saltation model performs, whether u_{*t} and c_o are universal and how they are
 308 probabilistically distributed must depend on the turbulent properties of saltation. As the JADE
 309 saltation fluxes are sampled at 1 Hz, we can use these data to examine (to some degree) the
 310 statistical behavior of saltation. In Fig. 4, the pdfs of the saltation fluxes for different particle
 311 size groups are plotted, computed using Q_{1sec} and Q_{1min} . It is seen that the pdfs generally behaves
 312 as

313

$$314 p(Q) \propto Q^{-\alpha} \quad (11)$$

315

316 In case of Q_{Isec} , there seems to be a distinct change in α at a critical value of $Q_c \sim 3 \text{ g m}^{-1} \text{ s}^{-1}$,
 317 with $\alpha \sim 1$ for $Q < Q_c$ and $\alpha \sim 4$ for $Q > Q_c$. The pdfs derived from Q_{Imin} appear to follow the
 318 basic functional form of Equation (11). Again, α is about 1 and tends to be larger for large Q
 319 values. Fig. 4 shows that the pdfs of Q depend significantly on the interval of time averaging,
 320 i.e., after averaging, smaller saltation fluxes become more frequent. This is because the time
 321 series of Q_{Isec} is more intermittent (see also Fig. 6).
 322



323
 324
 325 Figure 4: Probability density functions of Q_{Isec} (solid lines) and of Q_{Imin} (dashed lines) for four
 326 different particle sizes. Two additional lines $p(Q) \sim Q^{-1}$ and Q^{-4} are drawn as reference.
 327

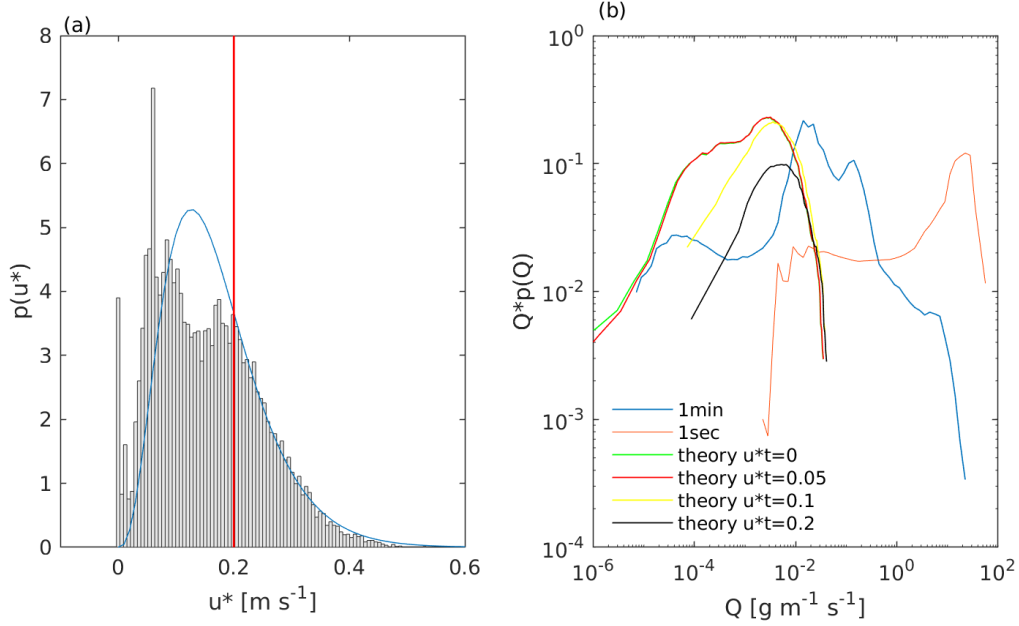
328 The pdfs of Q_{Isec} and Q_{Imin} integrated over all particles are shown in Figure 5b. Again, the pdfs
 329 show the general behavior of $p(Q) \sim Q^{-1}$. In theory, $p(Q)$ can be derived from the pdf of u_* ,
 330 $p(u_*)$. From Equation (2), we have
 331

$$332 \quad \frac{dQ}{du_*} = c_0 \frac{\rho}{g} (3u_*^2 + 2u_*u_{*t} - u_{*t}^2) \quad \text{for } u_* > u_{*t} \quad (12)$$

333
 334 This can be used to obtain
 335

$$336 \quad p(Q) = \begin{cases} p(u_*) \frac{du_*}{dQ} & \text{for } u_* > u_{*t} \\ 0 & \text{for } u_* \leq u_{*t} \end{cases} \quad (13)$$

337
 338 Fig. 5a shows the $p(u_*)$ estimated from u_{*Imin} together with the fitted Weibull distribution. For
 339 the fitting, emphasis is made to ensure that $p(u_*)$ for $u_* > 0.2 \text{ ms}^{-1}$ is best approximated. Fig. 5b
 340 shows the $p(Q)$ estimated from Q_{Imin} . We computed $p(Q)$ using Equation (13) with the fitted
 341 $p(u_*)$, assuming $u_{*t} = 0.2 \text{ ms}^{-1}$ and $c_0 = 2.6$. It is seen that the observed and modelled $p(Q)$ have
 342 qualitative similarities but using Equations (12) and (13) we cannot well reproduce the observed
 343 $p(Q)$. For example, the model fails to predict the lowly frequent strong saltation fluxes and the
 344 mode of saltation fluxes. Tests using several smaller u_{*t} values (0, 0.05 and 0.1) are also made.
 345 With smaller u_{*t} values, the mode of the predicted saltation fluxes is shifted to smaller values,
 346 but the predictions are far from satisfactory.
 347
 348



349
350

351 Figure 5: (a) Probability density functions of friction velocity, $p(u^*)$, plotted against u^* (bars).
352 To compute $p(u^*)$, u_{*1min} is used; a Weibull distribution (blue line) is fitted to $p(u^*)$; the red line
353 marks the assumed threshold friction velocity. (b) Probability density function of Q , in $Q^*p(Q)$,
354 estimated using Q_{1min} (blue) and Q_{1sec} (dark red) and using Equation (13) assuming several u^*t
355 values ($u^*t = 0.0 \text{ m s}^{-1}$, green; 0.05 m s^{-1} , red; 0.1 m s^{-1} , yellow; 0.2 m s^{-1} , black).
356

357 3.3 Saltation Intermittency

358

359 Following Stout and Zobeck [1997], the intermittency of saltation, γ , is defined as the fraction
360 of time during which saltation occurs at a given point in a given time period. It should be pointed
361 out that saltation intermittency describes only the behaviour of the process at $u^* \sim u^*t$, i.e.,
362 saltation intermittency is merely a special case of turbulent saltation. Several formulations of γ
363 are possible. Stout and Zobeck [1997] assumed that saltation occurs only in time windows when
364 u^* exceeds u^*t . Therefore, if $p(u^*)$ is known, then γ for a given u^*t can be estimated as
365

$$366 \gamma_a(u^*t) = 1 - \int_0^{u^*t} p(u_*) du_* \quad (14a)$$

367

368 Stout and Zobeck [1997] used the counts per second of sand impacts on a piezoelectric crystal
369 saltation sensor as a measure of saltation activity and found that γ_a rarely exceeded 0.5.

370

371 In Equation (14a) u^*t is fixed and thus saltation intermittency is attributed entirely to the
372 fluctuations of u^* . In reality, u^*t also fluctuates and satisfies certain pdfs [Raffaele et al., 2016].
373 In analogy to Equation (14a), γ for a given u^* can be estimated as
374

$$375 \gamma_b(u_*) = 1 - \int_{u_*}^{\infty} p(u^*t) du^*t \quad (14b)$$

376

377 More generally, we can define saltation intermittency as
378

$$379 \gamma_c = \int_0^{\infty} \left[1 - \int_0^{u^*t} p(u_*) du_* \right] p(u^*t) du^*t = \int_0^{\infty} \gamma_a(u^*t) p(u^*t) du^*t \quad (14c)$$

380

381 or

382

383
$$\gamma_c = \int_0^\infty \left[1 - \int_{u_*}^\infty p(u_{*t}) du_{*t} \right] p(u_*) du_* = \int_0^\infty \gamma_b(u_*) p(u_*) du_* \quad (14d)$$

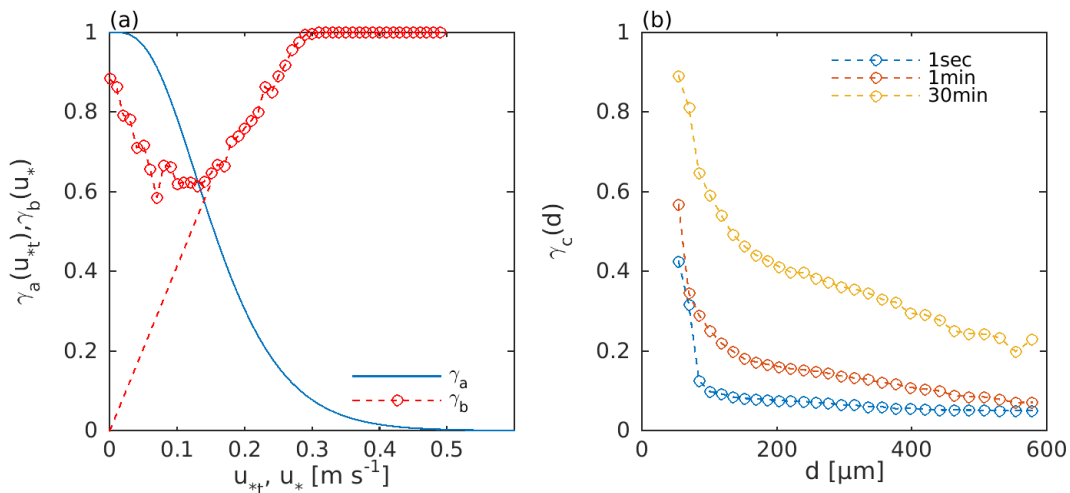
384

385 Equations (14c) and (14d) reduce to Equation (14a) if $p(u_{*t}) = \delta(u_{*t})$ and to Equation (14b)
 386 if $p(u_*) = \delta(u_*)$, respectively.

387

388 The computation of saltation intermittency function $\gamma_a(u_{*t})$ is done by integrating $p(u_*)$ (Fig. 5a)
 389 to fixed value of u_{*t} . In Fig. 6a, γ_a as function of u_{*t} is plotted. The behaviour of $\gamma_a(u_{*t})$ is as
 390 expected: it is one at $u_{*t} = 0$ and decreases to zero at about $u_{*t} = 0.5 \text{ ms}^{-1}$ as in the case of JADE,
 391 u_* rarely exceeded this value. For $u_{*t} = 0.2 \text{ ms}^{-1}$, γ_a is 0.35, comparable with the result of Stout
 392 and Zobeck [1997] who reported an intermittency of 0.4. As $p(u_{*t})$ is not known, Equation (14b)
 393 cannot be used directly, but we can compute $\gamma_b(u_*)$ using the JADE data. First, it is computed
 394 using Q_{1min} . This is done by selecting a fixed u_* say u_{*c} , and counting the time fraction, T_{u_*} ,
 395 which satisfies $|u_* - u_{*c}| < \varepsilon$ (used is $\varepsilon = 0.05 \text{ ms}^{-1}$) and the time fraction, T_{Q1min} , which
 396 satisfies $|u_* - u_{*c}| < \varepsilon$ and $Q_{1min} > 0$. By definition, saltation intermittency is T_{Q1min}/T_{u_*} as
 397 plotted in Fig. 6a. It is seen that for Q_{1min} , $\gamma_b(u_*)$ increases from about 0.6 at $u_* \sim 0.1 \text{ ms}^{-1}$ to
 398 about one at $u_* = 0.3 \text{ ms}^{-1}$. This shows that in JADE a considerable fraction of the saltation
 399 fluxes was recorded at u_* below the perceived threshold friction velocity (about 0.2 ms^{-1}),
 400 saltation is more intermit under weak wind conditions and becomes non-intermittent for $u_* >$
 401 0.3 ms^{-1} . The increase of $\gamma_b(u_*)$ with decreasing u_* for $u_* < 0.1 \text{ ms}^{-1}$ is however unexpected. The
 402 expected $\gamma_b(u_*)$ for small u_* is as depicted using the dashed line. A likely reason for the
 403 unexpected behaviour of $\gamma_b(u_*)$ is that during a wind erosion event, grains in saltation may
 404 continue to hop even when u_* is temporarily reduced to small values. The uncertainty in the
 405 data also needs to be considered, as the sample size for determining the ratio T_{Q1min}/T_{u_*} becomes
 406 smaller. More complete datasets are required to answer these questions. Finally, γ_c is computed
 407 by using Equation (14d) and is found to be around 0.73. For the one-second case, we cannot
 408 plot γ_b as a function of u_* , because u_* is not available at such high frequency. We computed γ_c
 409 for individual particle size groups (Fig. 6b) using Q_{1sec} , Q_{1min} and Q_{30min} , which is the time
 410 fraction of saltation for a given particle size, d , during the saltation event. It is found that $\gamma_c(d)$
 411 decreases with d , i.e., the saltation of larger particles is more intermittent. Also, $\gamma_c(d)$ increases
 412 with increased averaging time intervals, implying that the small scales features of turbulence
 413 play an important role in intermittent saltation.

414



415

416

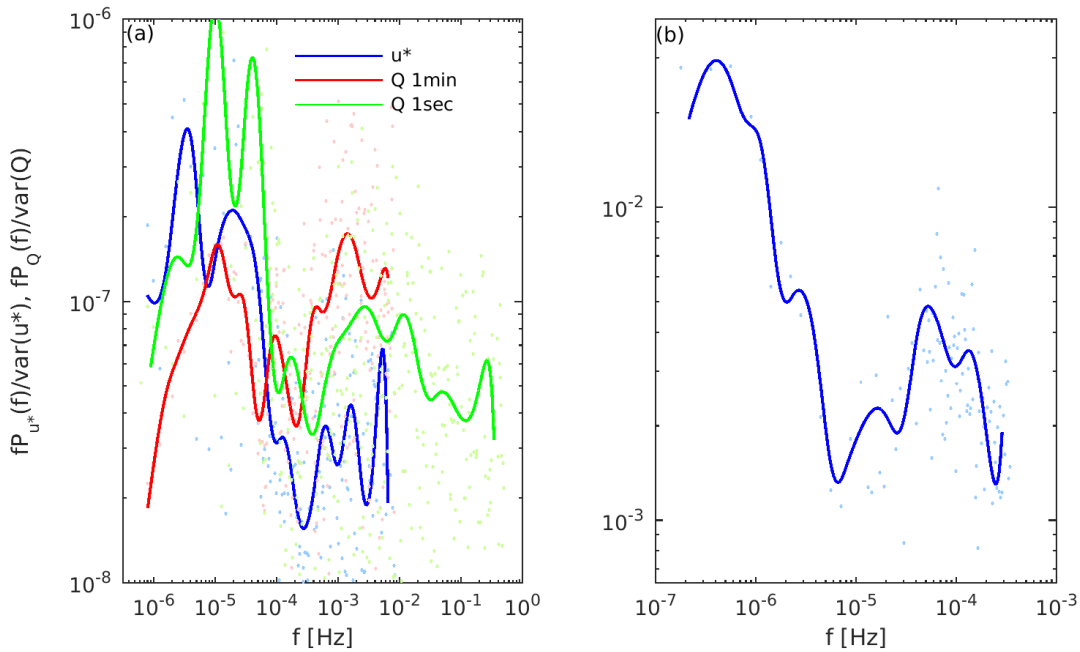
417 Figure 6: (a) Saltation intermittency function $\gamma_a(u_{*t})$, and $\gamma_b(u_*)$. See text for more details. (b) γ_c

418 as a function of particle size for Q_{1sec} , Q_{1min} and Q_{30min} .

419
 420
 421
 422
 423
 424
 425
 426
 427
 428
 429
 430
 431
 432
 433
 434
 435
 436
 437
 438
 439
 440
 441

3.4 Spectrum of Saltation Fluxes

Spectral analysis is a widely used for characterising the variations of a stochastic process on different scales. Using the JADE data, we computed the power spectrum of saltation fluxes, $P_Q(f)$ at frequency f , and of friction velocity, $P_{u^*}(f)$, using a non-uniform discrete Fourier transform. For comparison, the power spectra are normalized with the respective variances of the signal. In atmospheric boundary-layer studies, the spectra of various turbulence quantities have been thoroughly investigated (Stull, 1988). Examples for spectra of Reynolds shear stress can be found in McNaughton and Laubach (2000). Fig. 7 shows $P_Q(f)$ and $P_{u^*}(f)$ (Fig. 7a) as well their co-spectrum (Fig. 7b). $P_Q(f)$ is computed using both Q_{1sec} and Q_{1min} , and $P_{u^*}(f)$ with u^*_{1min} . It is seen that the power spectra of Q and u^* have qualitatively very similar behaviour. Both have a maximum at about 10^{-5} Hz, a minimum at about 10^{-4} Hz and another peak at about 2×10^{-3} Hz. The maximum at 10^{-5} Hz is related to the diurnal patterns and changing synoptic events, which drive the wind erosion episodes, the minimum at 10^{-4} Hz is due to the lack of turbulent winds at the time scale of several hours, while the peak at 2×10^{-3} Hz is caused by the minute-scale gusty winds/large eddies in turbulent flows. Also the Q - u^* co-spectrum shows that Q and u^* are most strongly correlated on diurnal/synoptic and gust/large-eddy time scales. $P_Q(f)$ computed using Q_{1sec} reveals again the peaks at 10^{-5} Hz and at 2×10^{-3} Hz. The power of the Q spectrum then decreases with frequency. As the sampling rate of saltation flux is limited to one second in this study, the features of $P_Q(f)$ at frequencies larger than 0.5 Hz are not resolved.



442
 443
 444
 445
 446
 447
 448
 449

Figure 7: (a) Normalized power spectrum of u^* (blue) computed with u^*_{1min} , together with the normalized power spectrum of saltation flux computed with Q_{1min} (red) and Q_{1sec} (green). (b) Normalized Q - u^* co-spectrum, computed using with Q_{1min} and u^*_{1min} . In both (a) and (b), dots are unsmoothed spectra, and curves are smoothed spectra.

4. Estimates of Saltation Model Parameters

450 Given the turbulent nature of saltation, it is rational to treat u_{*t} and c_0 in the saltation model as
 451 parameters obeying certain probability distributions. To examine the behavior of these
 452 parameters, we introduce two coefficients r_{c0} and $r_{u_{*t}}$, and multiply them respectively by the
 453 “theoretical” values of c_0 and u_{*t} in Equation (2), i.e.

454

$$u_{*t} = r_{u_{*t}} u_{*t, theory}$$

455

$$c_0 = r_{c0} c_{0, theory}$$

456

457 As introduced in Section 1, we assumed $c_{0, theory} = 2.6$ and computed $u_{*t, theory}$ using Equation (1)
 458 with observed soil moisture and fraction of cover. The two coefficients r_{c0} and $r_{u_{*t}}$ are varied to
 459 generate a model estimate of Q using Equations (2) and (3) with observed u_{*t} . The probability
 460 distributions of r_{c0} and $r_{u_{*t}}$ are estimated using the following techniques. Let us denote the time
 461 series of the modelled saltation flux as $Q_{M,i}$ ($i=1, N$) and of the corresponding measurement $Q_{D,i}$.
 462 The absolute error, δQ_A , and Nash coefficient, I_{Nash} , are used as measures for the goodness of
 463 the agreement between the model and the measurement. They are defined as,

464

$$465 \quad \delta Q_A = \frac{1}{N} \sum |a_i|$$

$$466 \quad I_{Nash} = (1 - \sum a_i^2 / \sum b_i^2)$$

467

468 with

469

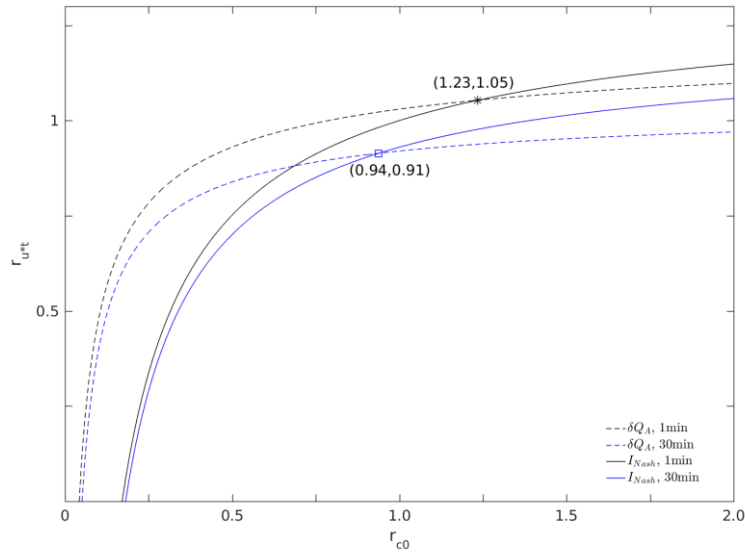
$$a_i = Q_{M,i} - Q_{D,i}$$

$$470 \quad b_i = Q_{M,i} - \frac{1}{N} \sum Q_{M,i}$$

$$c_i = \begin{cases} a_i / Q_{M,i} & Q_{M,i} \neq 0 \\ 0 & \text{else} \end{cases}$$

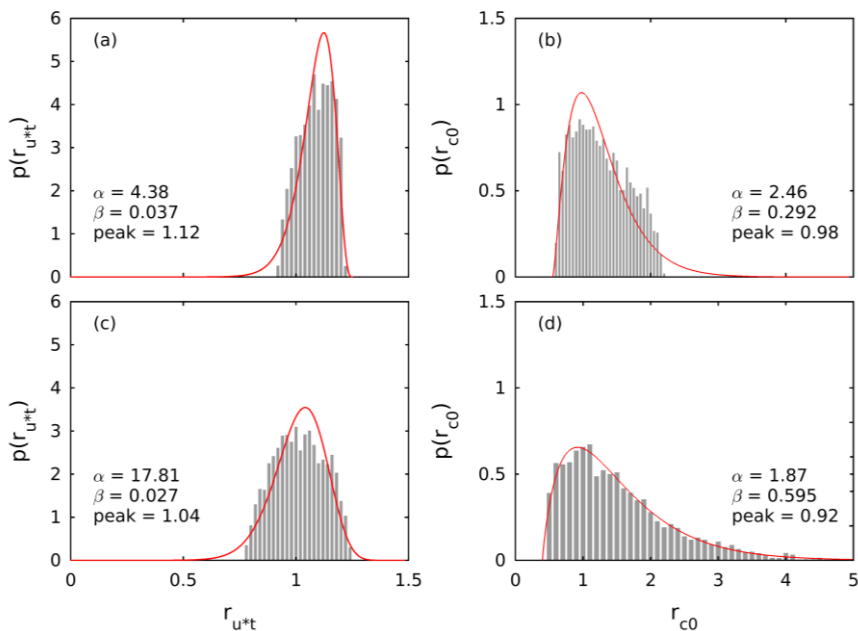
471

472 The prior pdfs of r_{c0} and $r_{u_{*t}}$ are assumed to be uniform. In the numerical experiment, we
 473 randomly generate r_{c0} and $r_{u_{*t}}$ and seek their values, such that $\delta Q_A \leq \varepsilon$ and $I_{Nash} > \eta$. These
 474 experiments are repeated for Q_{1min} and Q_{30min} . The plots of δQ_A and I_{Nash} as functions of r_{c0} and
 475 $r_{u_{*t}}$ show that for certain values of r_{c0} and $r_{u_{*t}}$, the above conditions are satisfied. Fig. 8 shows
 476 that for Q_{1min} , the best simulation is achieved with $r_{c0} = 1.23$ and $r_{u_{*t}} = 1.05$, while for the Q_{30min} ,
 477 with $r_{c0} = 0.94$ and $r_{u_{*t}} = 0.91$. This suggest that the “optimal” estimates of u_{*t} and c_0 are close
 478 to the corresponding theoretic values, but are dependent on the time averaging intervals, with
 479 both u_{*t} and c_0 being larger for shorter averaging intervals.



480
 481 Figure 8: δQ_A and I_{Nash} are both functions of r_{c0} and r_{u^*t} . Along the dashed curves, the
 482 condition $\delta Q_A = \min$ is satisfied and along the solid curves the condition $I_{Nash} = \max$ is
 483 satisfied. The curves are estimated with both Q_{1min} and Q_{30min} .
 484

485 The parameter pdfs $p(r_{u^*t})$ and $p(r_{c0})$ are estimated with the DREAM algorithm, again using the
 486 absolute error and the Nash coefficient as goodness of agreement between the model simulated
 487 and measured saltation fluxes. The results are shown in Fig. 9. All pdfs are fitted to a Γ -
 488 distribution. As seen in Fig. 9a and 9c, the most frequent r_{u^*t} values are respectively 1.12 and
 489 1.04 for Q_{1min} and Q_{30min} , close to the estimates of 1.05 and 0.91 found in Fig. 8. For Q_{1min} , r_{u^*t}
 490 is $\sim 1.12 \pm 0.2$ and for Q_{30min} $\sim 1.04 \pm 0.3$. This implies that sometimes saltation occurs when u^*
 491 is below the theoretical u^*t value and sometimes saltation does not occur even when u^* is above
 492 it, as already seen in Fig. 6a. In the case of $p(r_{c0})$ (Fig. 9c and 9d), the most frequent values of
 493 r_{c0} for Q_{1min} and Q_{30min} are, respectively, 1.04 and 0.92, close to the optimal estimates of 1.23
 494 and 0.94 shown in Fig. 8. But r_{c0} varies over a wide range, for instance, for Q_{30min} between 0.5
 495 and 5, i.e., c_0 is a rather stochastic parameter.
 496



498 Figure 9: (a) Parameter pdf $p(r_{u^*t})$ for 1-min averaged saltation fluxes; (b) as (a), but for $p(r_{c0})$;
499 (c) and (d), as (a) and (b), but for 30-min averaged saltation fluxes.

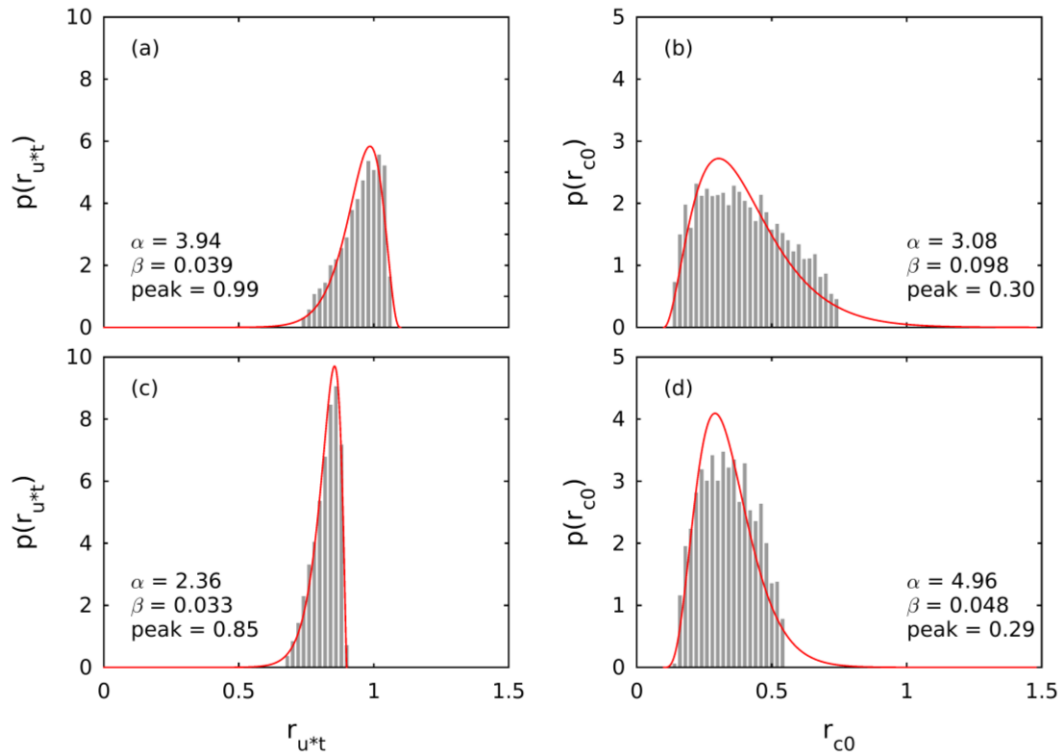
500

501 In nature, many factors influence sediment transport, but the stochasticity of the parameters is
502 determined primarily by the turbulent fluctuations of friction velocity (or surface shear stress),
503 the randomness of threshold friction velocity, and soil particle size distribution (representing
504 particle response to forcing). Studies have shown, for instance, that small changes in soil
505 moisture can have large influences on saltation [Ishizuka et al. 2008] and soil moisture in the
506 very top soil layer can vary significantly over relatively short time periods. Over the period of
507 18 days during JADE soil moisture in the top 0.05 m layer varied between 0.02 and 0.04 m^3m^{-3}
508 ³ (4 and 8% in relative soil moisture, assuming a saturation soil moisture of 0.5 m^3m^{-3}). In this
509 study, the influence of soil moisture on saltation is accounted for via Equation (1) using the soil
510 moisture measurements in the top 0.05m layer (see also Fig. 4a in Shao et al. 2011). While
511 measured soil moisture is used in the wind erosion model, the randomness associated with its
512 spatial-temporal variations is not, which is most likely reflected in the stochasticity of u^*_{t} .

513

514 The stochasticity of c_0 arises because saltation fluctuates, depending on turbulence and particle
515 size. To demonstrate this, we divided the time series of the saltation fluxes into two subsets,
516 one with $Q_{D,i} \leq 3 \text{ g m}^{-1} \text{ s}^{-1}$ representing weak saltation and one with $Q_{D,i} > 3 \text{ g m}^{-1} \text{ s}^{-1}$ representing
517 significant saltation. This separation is arbitrary but sufficient for making the point that c_0
518 depends on u^* , also a measure of turbulence intensity. The parameter pdfs, $p(r_{u^*t})$ and $p(r_{c0})$, for
519 the subset $Q_{D,i} \leq 3 \text{ g m}^{-1} \text{ s}^{-1}$ is shown in Fig. 10. For Q_{1min} and Q_{30min} , the most frequent r_{u^*t}
520 values are now respectively 0.99 and 0.85, somewhat smaller than the estimated values for the
521 full set (Fig. 9). In comparison, the most frequent r_{c0} values are now respectively 0.30 and 0.29,
522 three to four times smaller than for the case when the full set is considered (Fig. 9). This
523 suggests that c_0 has a clear dependency on u^* and is smaller for smaller u^* . This is because
524 saltation is more intermittent in the case of smaller u^* (i.e. smaller excess shear stress) and thus,
525 c_0 , a descriptor of the relation between time-averaged saltation flux and friction velocity, is
526 smaller for more intermittent saltation.

527



528
 529 Figure 10: As Fig. 9, but estimated using the time series of saltation fluxes which satisfy $Q_{D,i} \leq$
 530 $3 \text{ g m}^{-1} \text{ s}^{-1}$.
 531

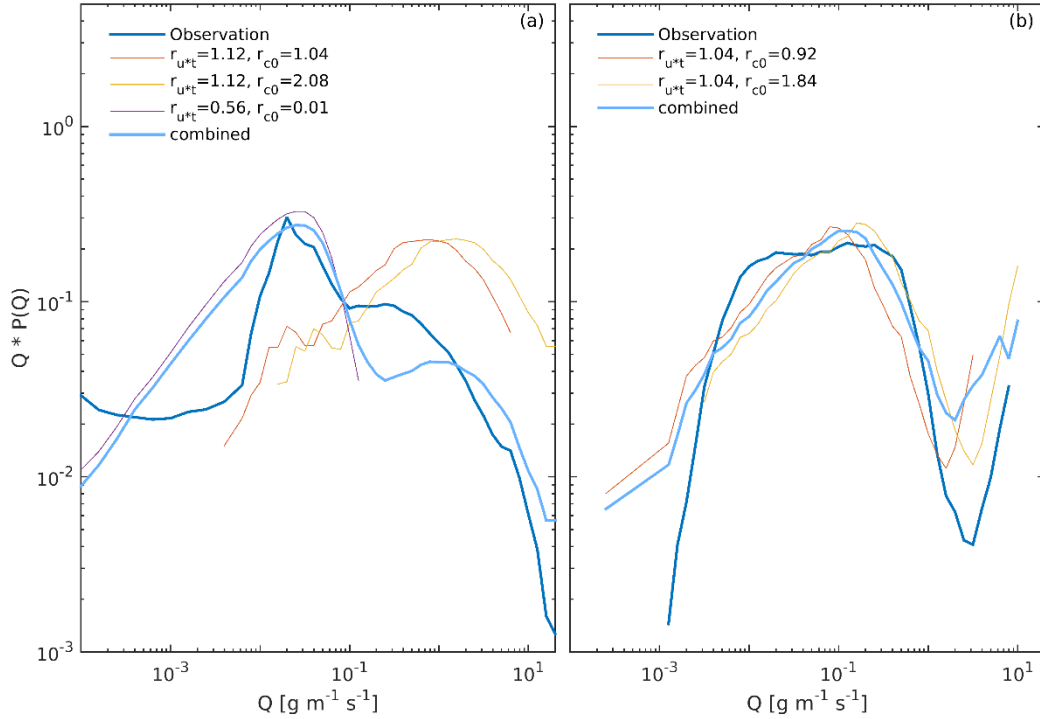
532 We fit the pdfs, $p(r_{u*})$ and $p(r_{c0})$, for individual particle size bins and found that the most
 533 frequent r_{u*} values do not differ substantially among the particle sizes, but r_{c0} depends
 534 systematically on particle size. For example, the most frequent r_{c0} values for 101, 151, 203, 315
 535 and 398 μm are, respectively, 0.5, 1.3, 1.7, 3.1 and 4.0. These values are obtained by first
 536 estimating $p(r_{c0})$ for the individual particle size bins with the measured saltation flux for the
 537 corresponding bins and then normalizing $p(r_{c0})$ with the mass fraction of the size bins of the
 538 parent soil. A least squares curve fitting shows that the most frequent r_{c0} value depends almost
 539 perfectly ($R^2 = 0.996$) linearly on particle size:

$$541 \quad r_{c_0} = 0.012d - 0.59 \quad (15)$$

542
 543 for the particle size range (100 to 400 μm) we tested, with d being particle size in μm .
 544

545 We have shown that both u_{*t} and c_0 satisfy certain pdfs that depend on the properties of the
 546 surface, atmospheric turbulence and soil particle size. Fig. 9 shows that for a fixed choice of u_{*t}
 547 and c_0 , even if they are “optimally” chosen, a portion of the measurements cannot be
 548 represented by the model. Then, how does the saltation model perform if a single fixed u_{*t} and
 549 a single fixed c_0 are used as is often the case in aeolian models? The $p(Q)$ computed using the
 550 model and derived from the JADE measurements are shown for Q_{1min} and Q_{30min} in Fig. 11. The
 551 model is applied to estimate the saltation flux for individual particle size groups using the
 552 optimally estimated u_{*t} and c_0 (with $r_{u*} = 1.12$ and $r_{c0} = 1.04$ for Q_{1min} , and $r_{u*} = 1.04$ and r_{c0}
 553 $= 0.92$ for Q_{30min}) and the total saltation flux is computed by integration over all particle size
 554 groups, i.e., using Equation (3). Fig. 11 shows that for this option, the model over predicts the
 555 probability of large Q , but under predicts the probability of small Q , in both cases of Q_{1min} and
 556 Q_{30min} . Obviously, to better reproduce the Q_{1min} and Q_{30min} pdfs, more values of r_{u*} and r_{c0}
 557 sampled from the parameter pdfs are required. We have therefore modelled Q_{1min} with other

558 choices of r_{u^*t} (1.12 and 0.56) and r_{c0} (2.08, 0.01) and plotted the corresponding Q_{1min} pdfs as
 559 well as the averaged Q_{1min} pdf of the three simulations. Similarly, we performed Q_{30min} model
 560 simulations with other r_{u^*t} (1.04) and r_{c0} (1.84) values and examined the Q_{30min} pdfs. With the
 561 additional choices of the r_{u^*t} and r_{c0} values, the Q_{1min} and Q_{30min} pdfs can be better reproduced.
 562



563
 564 Figure 11: (a) Probability density functions of observed Q and simulated Q for 1-min averages
 565 with several choices of r_{u^*t} and r_{c0} ; (b) as (a), but for 30-min averages.
 566

567 5. Summary

568
 569 In this paper, we used the JADE data of saltation fluxes (resolution one second) and frictional
 570 velocity (resolution one minute) to analyze the statistical behavior of turbulent saltation and
 571 estimate the probability distribution of two important parameters in a saltation model, namely,
 572 the threshold friction velocity, u^*t , and saltation coefficient, $c0$.
 573

574 Saltation fluxes show rich variations on different scales. It is found that while the widely used
 575 $Q \sim u^{*3}$ relationship holds in general, it can vary significantly between different wind erosion
 576 events. In several wind erosion events observed in JADE, saltation hysteresis occurred. We
 577 examined the probability density function of the saltation fluxes, $p(Q)$, and found that it
 578 generally behaves like $Q^{-\alpha}$ with $\alpha \sim 1$. For Q_{1sec} , there is a distinct change in α at $Q = 3 \sim 4 \text{ g m}^{-1}$
 579 s^{-1} with $\alpha \sim 1$ for smaller Q and $\alpha \sim 4.0$ larger Q . It is shown that $p(Q)$ is dependent on the
 580 averaging time intervals as a consequence of saltation intermittency.
 581

582 We introduced the saltation intermittency functions $\gamma_a(u^*t)$, $\gamma_b(u^*)$ and redefined saltation
 583 intermittency γ_c as the fraction of time during which saltation occurs at a given point in a given
 584 time period, and computed these saltation intermittency measures using the JADE saltation flux
 585 measurements. It is found that $\gamma_a(u^*t)$ is one at $u^*t = 0$ and decreases to zero at about $u^*t = 0.5$
 586 ms^{-1} . For $u^*t = 0.2 \text{ ms}^{-1}$, γ_a is 0.35. For Q_{1min} , $\gamma_b(u^*)$ increases from about 0.6 at $u^* \sim 0.1 \text{ ms}^{-1}$
 587 to about one at $u^* = 0.3 \text{ ms}^{-1}$. This shows that a considerable fraction of the saltation fluxes
 588 occurs at small friction velocity and saltation is more intermittent under weak wind conditions

589 and is almost non-intermittent for $u_* > 0.3 \text{ m s}^{-1}$. It is found that $\gamma_b(u_*)$ increased with decreasing
590 u_* for $u_* < 0.1 \text{ ms}^{-1}$ which is unexpected. Overall, γ_c is found to be around 0.73. We computed
591 γ_c as function of particle size and found that $\gamma_c(d)$ decreases with d , i.e., the saltation of larger
592 particles is more intermittent. Also, $\gamma_c(d)$ increases with increased averaging time intervals,
593 implying that the small scales features of turbulence play an important role in intermittent
594 saltation.

595
596 The power spectra of Q and u_* are found to have qualitatively similar behaviour. Both have a
597 maximum at about 10^{-5} Hz , a minimum at about 10^{-4} Hz and another peak at about $2 \times 10^{-3} \text{ Hz}$.
598 The maximum at 10^{-5} Hz is related to the diurnal to synoptic events that drive wind erosion
599 episodes, the minimum at 10^{-4} Hz is due to the lack of turbulent wind fluctuations at the time
600 scale of several hours, while the peak at $2 \times 10^{-3} \text{ Hz}$ is caused by minute-scale gusts/large eddies
601 in turbulent flows. The power of the saltation rapidly decreases with frequency and becomes
602 relatively weak at frequencies of 0.1 Hz .

603
604 The posterior pdfs of the two parameters were estimated using the DREAM algorithm applied
605 to the JADE saltation flux measurements. While both u_{*t} and c_0 have clear physical
606 interpretations, they are both stochastic parameters satisfying certain parameter pdfs. They also
607 dependent on the intervals of time averaging. Both u_{*t} and c_0 for Q_{1min} are larger than for Q_{30min} .
608 The pdf of u_{*t} shows that it has a most frequent value close to the theoretical value, but can vary
609 over a range of 20% to 30%. The pdf of c_0 shows scatter over a wide range and it is unlikely
610 that a universal c_0 exists. In a saltation model, even if the optimally estimated c_0 is used,
611 considerable scatter between the model and the data would remain. The likely reason for the
612 stochasticity in u_{*t} may be the temporal and spatial variations of particle cohesion, surface
613 roughness, particle shape etc. which cannot be well represented by a fixed deterministic value,
614 and the relatively large uncertainty in c_0 may be that this parameter depends on additional
615 factors (e.g. u_* and soil particle size distribution) and is related to the fluctuations and
616 intermittency of saltation. It may also be that saltation in reality is never in equilibrium as
617 Bagnold [1941], Kawamura [1964] and Owen [1964] conceptualized, because due to turbulence,
618 sand grains are continuously entrained at different rates into the airflow and a continuous flow-
619 and particle-motion feedback takes place. As a consequence, it is difficult to treat c_0 as a
620 universal constant.

621
622 In this study, we highlighted the need to better understand saltation as a turbulent process and
623 the stochasticity of saltation model parameters. The concept of threshold friction velocity as a
624 stochastic variable was put forward in Shao [2001]. Raffaele et al. [2016] examined the pdf of
625 u_{*t} using data compiled from publications. Raffaele et al. [2018] studied how u_{*t} uncertainties
626 propagate in saltation flux calculations and reported that in the case of small excess shear stress,
627 all models they tested amplify the uncertainty in estimated saltation flux, especially for coarse
628 sand. This finding is consistent with our notion that c_0 also is a stochastic variable. Due to the
629 stochasticity of the model parameters, the saltation model cannot reproduce the observation
630 even with the optimally estimated parameters (e.g. under estimation of weak saltation fluxes
631 and over estimation of strong saltation fluxes). A combination of several pairs of model
632 parameters appears to be required to reasonably reproduce the pdfs of saltation fluxes.

633
634 Our estimates of the parameter uncertainties is based on the data of a relatively simple aeolian
635 surface. For more complex surfaces, we expect the parameter uncertainties to be even more
636 pronounced.
637

638 **Acknowledgement:** This research is funded by the National Natural Science Foundation of
639 China (No. 41571090, 41201539). The data used in this study were obtained in JADE (the Japan
640 Australian Dust Experiment) by M. Ishizuka, M. Mikami, J. F. Leys, Y. Yamada, and S.
641 Heidenreich. We are grateful to P. Schlüter and Q. Xia for support with data processing. We
642 also wish to thank Dr. J. Gillies, Dr. M. Klose and an anomalous referee for their helpful
643 comments which prompt us to rework on a number of issues presented in the first version of
644 the paper.

645
646 **References:**

- 647
648 Anderson, R. S. and P. K. Haff (1988): Simulation of Eolian Saltation. *Science* 241, 820-823.
649 DOI: [10.1126/science.241.4867.820](https://doi.org/10.1126/science.241.4867.820)
- 650 Bagnold, R.A. (1941): *The Physics of Blown Sand and Desert Dunes*. Methuen, London, 265pp
651
- 652 Butterfield, G. R. (1991): Grain transport rates in steady and unsteady turbulent airflows. *Acta*
653 *Mechanica*, Suppl. 1, 97-122
- 654
655 Davidson-Arnott, R. G. D., and B. O. Bauer (2009): Aeolian sediment transport on a beach:
656 Thresholds, intermittency, and high frequency variability. *Geomorphology* 105: 117–126
657
- 658 Dupont, S., G. Bergametti, B. Marticorena, and S. Simoëns (2013), Modeling saltation
659 intermittency, *J. Geophys. Res. Atmos.*, 118, 7109–7128, doi:10.1002/jgrd.50528
660
- 661 Ellis, J. T., D. Sherman, E. J. Farrell and B. L. Li (2012): Temporal and spatial variability of
662 aeolian sand transport: Implications for field measurements. *Aeolian Research* 3(4):379-387.
663 DOI: [10.1016/j.aeolia.2011.06.001](https://doi.org/10.1016/j.aeolia.2011.06.001)
664
- 665 Fecan, F., Marticorena B., Bergametti G. (1999) Parametrization of the increase of the aeolian
666 erosion threshold wind friction velocity due to soil moisture for arid and semi-arid areas.
667 *Annales Geophysicae* 17:149–157
668
- 669 Gillette, D.A., E. Hardebeck and J. Parker (1997) Large-scale variability of wind erosion mass
670 flux rates at Owens Lake 2. Role of roughness change, particle limitation, change of threshold
671 friction velocity, and the Owen effect. *J. Geophys. Res.* 102, 25,989-25,998
672
- 673 Ishizuka, M., Mikami, M., Leys, J. F., Yamada, Y., Heidenreich, S., Shao, Y., McTainsh, G. H.
674 (2008): Effects of soil moisture and dried raindroplet crust on saltation and dust emission. *J.*
675 *Geophys. Res.* 113, D24212, doi:10.1029/2008JD009955
676
- 677 Ishizuka, M., Mikami, M., Leys, J. F., Shao, Y., Yamada, Y. and Heidenreich, S. (2014): Power
678 law relation between size-resolved vertical dust flux and friction velocity measured in a fallow
679 wheat field. *Aeolian Research* 12:87-99. DOI: [10.1016/j.aeolia.2013.11.002](https://doi.org/10.1016/j.aeolia.2013.11.002)
680
- 681 Klose, M., Y. Shao, X. Li, H. Zhang, M. Ishizuka, M. Mikami, and J. F. Leys (2014): Further
682 development of a parameterization for convective turbulent dust emission and evaluation based
683 on field observations. *J. Geophys. Res. Atmos.* 119, 10,441–10,457,
684 doi:[10.1002/2014JD021688](https://doi.org/10.1002/2014JD021688)
685

686 Kok, J.F., N.M. Mahowald, G. Fratini, J.A. Gillies, M. Ishizuka, J.F. Leys, M. Mikami, M.S.
687 Park, S.U. Park, R.S. Van Pelt, T.M. Zobeck (2014): An improved dust emission model – Part
688 1: model description and comparison against measurements. *Atmos. Chem. Phys.* 14, 13023–
689 13041

690
691 Kawamura, R. (1964): Study of sand movement by wind. In: *Hydraulic Eng. Lab. Tech. Rep.*,
692 University of California, Berkeley, HEL-2-8, pp 99–108

693
694 Leys, J. F. (1998): Wind erosion processes and sediments in southeastern Australia. Ph.D.
695 Thesis, Griffith University, Brisbane

696
697 Namikas, S. L., B. O. Bauer and D. Sherman (2003): Influence of averaging on shear velocity
698 estimates for aeolian transport modeling. *Geomorphology* 53, 235-246, DOI: 10.1016/S0169-
699 555X(02)00314-8

700
701 McKenna-Neuman, C., N. Lancaster, and W. G. Nickling (2000): The effect of unsteady winds
702 on sediment transport on the stoss slope of a transverse dune, Silver Peak, NV, USA.
703 *Sedimentology* 47: 211–226

704
705 McNaughton, K. G. and J. Laubach (2000): Power Spectra and Cospectra for Wind and For
706 Wind and Scalars in a Disturbed Surface Layer at the Base of an Advective Inversion.
707 *Boundary-Layer Meteorology* 96: 143–185.

708
709 Owen, R. P. (1964): Saltation of uniform grains in air. *J. Fluid. Mech.* 20, 225–242

710
711 Raffaele, L., L. Bruno, F. Pellerey and L. Preziosi, 2016: Windblown sand saltation: A
712 statistical approach to fluid threshold shear velocity. *Aeolian Research* 23, 79–91,
713 <http://dx.doi.org/10.1016/j.aeolia.2016.10.002>

714
715 Raffaele, L., L. Bruno and G.F.S. Wiggs, 2018: Uncertainty propagation in aeolian processes:
716 From threshold shear velocity to sand transport rate. *Geomorphology*,
717 <https://doi.org/10.1016/j.geomorph.2017.10.028>

718
719 Raupach, M.R., Gillette D.A. and Leys J.F. (1993): The effect of roughness elements on wind
720 erosion thresholds. *J. Geophys. Res.* 98:3023–3029

721
722 Sadegh, M. and J. A. Vrugt (2014): Approximate Bayesian computation using Markov Chain
723 Monte Carlo simulation: DEARM_(ABC). *Water Resour. Res.* 50, doi:10.1002/2014WR015386

724
725 Shao, Y. and Lu H. (2000): A simple expression for wind erosion threshold friction velocity. *J.*
726 *Geophys. Res.* 105:22,437–22,443

727
728 Shao, Y. (2001): *Physics and Modelling of Wind Erosion*. 1st Edition, Kluwer Academic
729 Publishers.

730
731 Shao, Y., M. Ishizuka, M. Mikami, and J. F. Leys (2011): Parameterization of size-resolved
732 dust emission and validation with measurements. *J. Geophys. Res.*, 116, D08203,
733 doi:[10.1029/2010JD014527](https://doi.org/10.1029/2010JD014527)

734

735 Shao, Y. and Mikami, M. (2005): Heterogeneous Saltation: Theory, Observation and
736 Comparison. *Boundary-Layer Meteorol.* 115:359. doi:10.1007/s10546-004-7089-2
737
738 Sherman, D., B. L. Li, J. T. Ellis and C. Swann (2017): Intermittent aeolian saltation: A protocol
739 for quantification. *Geographical Review* 1–19. DOI: 10.1111/gere.12249
740
741 Storn, R. and Price, K. (1997): Differential Evolution – a simple and efficient heuristic for
742 global optimization over continuous spaces. *J. Global Optim.* 11, 341-359
743
744 Stout, J. E. and T. M. Zobeck (1997): Intermittent saltation. *Sedimentology* 44, 959-970
745
746 Stull, R. B. (1988): *An Introduction to Boundary Layer Meteorology*. Kluwer Academic
747 Publishers.
748
749 Vrugt, J. A., ter Braak, C. J. F., Diks, G. H., Robinson, B. A., and Hyman, J. M. (2011):
750 Accelerating Markov Chain Monte Carlo Simulation by Differential Evolution with Self-
751 Adaptive Randomized Subspace Sampling. *Int. J. Nonlin. Sci. Num.* 10(3), 273-
752 290doi:10.1515/IJNSNS.2009.10.3.273
753
754 Vrugt, J. A. and M. Sadegh (2013): Toward diagnostic model calibration and evaluation:
755 Approximate Bayesian computation. *Water Resour. Res.* 49, 4335-4345.
756 doi:10.1002/wrcr.20354
757
758 White, B.R. (1979): Soil transport by winds on Mars. *J. Geophys. Res.* 84, 4643-4651
759
760 Yamada Y., Mikami M., Nagashima H. (2002): Dust particle measuring system for streamwise
761 dust flux. *J. Arid Land Studies* 11(4): 229–234